The Company of Biologists

RESEARCH ARTICLE

Integrating gastrocnemius force–length properties, *in vivo* activation and operating lengths reveals how *Anolis* deal with ecological challenges

Kathleen L. Foster*,‡ and Timothy E. Higham

ABSTRACT

A central question in biology is how animals successfully behave under complex natural conditions. Although changes in locomotor behaviour, motor control and force production in relation to incline are commonly examined, a wide range of other factors, including a range of perch diameters, pervades arboreal habitats. Moving on different substrate diameters requires considerable alteration of body and limb posture, probably causing significant shifts in the lengths of the muscle–tendon units powering locomotion. Thus, how substrate shape impacts *in vivo* muscle function remains an important but neglected question in ecophysiology. Here, we used high-speed videography, electromyography, *in situ* contractile experiments and morphology to examine gastrocnemius muscle function during arboreal locomotion in the Cuban knight anole, *Anolis equestris*. The gastrocnemius contributes more to the propulsive effort on broad surfaces than on narrow surfaces. Surprisingly, substrate inclination affected the relationship between the maximum potential force and fibre recruitment; the trade-off that was present between these variables on horizontal surfaces became a positive relationship on inclined surfaces. Finally, the biarticular nature of the gastrocnemius allows it to generate force isometrically, regardless of substrate diameter and incline, despite the fact that the tendons are incapable of stretching during cyclical locomotion. Our results emphasize the importance of considering ecology and muscle function together, and the necessity of examining both mechanical and physiological properties of muscles to understand how animals move in their environment.

KEY WORDS: Muscle function, *Anolis equestris*, Arboreality, Electromyography, Tendon, *In situ* force–length curve

INTRODUCTION

How animals function in their environment determines their performance at numerous tasks that are integral for survival (Foster et al., 2015; Irschick and Higham, 2016). The majority of these tasks, such as evading predators and capturing prey, require locomotion in highly heterogeneous environments. The neuromuscular system, fundamental for powering locomotion, must, therefore, exhibit enough morphological, behavioural and/or

Department of Biology, University of California, 900 University Avenue, Riverside, CA 92521, USA.
*Present address: Department of Biology, University of Ottawa, 30 Marie Curie, Ottawa, ON, Canada K1N 7N1.

‡Author for correspondence (kfost001@ucr.edu)

K.L.F., 0000-0002-7365-7885

physiological flexibility to generate movement in the face of these varying conditions.

Muscle function can shift to allow animals to meet environmental demands over short time scales or through evolutionary changes in morphology. For example, muscle moment arms are greater for those species that commonly move on steep inclines (Zaaf et al., 1999; Herrel et al., 2008a,b), and muscles have longer fibres in species that rely on locomotor behaviours that require large limb oscillations (Loeb and Gans, 1986; Biewener, 1998; Biewener and Gillis, 1999; Daley and Biewener, 2003). Although the time scale of such changes in morphology may be long, short-term alterations in muscle activation and operating length can alter muscle force production. Muscle recruitment may increase to meet an increased demand for muscle work (e.g. on an incline; Carlson-Kuhta et al., 1998; Gillis and Biewener, 2002; Daley and Biewener, 2003; Higham and Jayne, 2004; Foster and Higham, 2014) or the lengths over which the muscle is generating force can change, impacting the amount of force and/or work it generates because of where it is active on its force–length and/or force–velocity curves (e.g. Johnston, 1991; Roberts et al., 1997; Olson and Marsh, 1998; Gabaldón et al., 2004). Integrative studies examining the plasticity of neuromuscular function with changes in habitat structure often focus on incline, but multiple things are likely to be changing simultaneously, such as both perch diameter and incline. This is especially the case for arboreal vertebrates.

Anolis are arboreal lizards that have repeatedly and rapidly evolved ecomorphs that differ morphologically and behaviourally based on the region of the arboreal environment in which they specialize (Losos, 1994, 2009). They are extremely adept at moving through the highly complex arboreal environment, and the shifts in limb kinematics required for these animals to move on different arboreal surfaces, particularly different diameter perches (Spezzano and Jayne, 2004; Foster and Higham, 2012), suggest that shifts in motor recruitment (Foster and Higham, 2014) and/or operating lengths will be necessary for the maintenance of a given amount of force. Although motor control has been examined recently (Foster and Higham, 2014), other important aspects of muscle function (i.e. force production) have been neglected. This is probably due to the relatively small body size of *Anolis*, which precludes *in vivo* measurements of muscle force.

Tendons can transfer force and store elastic energy via stretch and recoil. However, small animals cannot take advantage of the latter because there is insufficient time to employ a catch mechanism and the muscle forces and body mass are too small to deform the tendon without a catch mechanism (Biewener et al., 1981; Biewener and Blickhan, 1988; Pollock and Shadwick, 1994b; Astley and Roberts, 2012). If tendons are incapable of deforming during cyclical, non-ballistic locomotion in *Anolis* lizards, then *in vivo* muscle length can be inferred from 3D joint kinematics, as is done for fishes (Katz and

Shadwick, 1998; Shadwick et al., 1998; Donley and Shadwick, 2003). *In vivo* muscle activation patterns and 3D joint kinematics could then be linked to *in situ* force–length contractile properties.

We first used the muscle and tendon of the gastrocnemius in *Anolis equestris* to test whether tendons are capable of deformation during cyclical locomotion using calculations based on dissections of hindlimb muscles and tendons as well as evidence derived from *in situ* contractile experiments. Then, we combined 3D locomotor kinematics, *in vivo* muscle activation data and *in situ* force–length properties to determine whether the gastrocnemius of small arboreal animals operates at or near the plateau of the force–length curve (FLC) and how its function shifts in the face of changes in environmental demand.

The geometry of a broad surface means the position of the foot (on top of the surface rather than on the side) should allow ankle extension to contribute more to propulsion than it would on a narrow surface (Foster and Higham, 2014). Therefore, we predicted that, on broad surfaces, this greater propulsive contribution will occur via increased gastrocnemius motor unit recruitment, activity occurring at a length that results in greater force (i.e. optimal position on the FLC), or a combination of the two. Further, we expected to see a trade-off between potential force (force predicted by the *in situ* FLC) and muscle recruitment. We tested these predictions using a combination of high-speed videography, electromyography, *in situ* experiments and anatomical dissections.

MATERIALS AND METHODS

Seven adult male *Anolis equestris* Merrem 1820 (mass 58.5±5.8 g; snout–vent length, SVL 14.3±0.5 cm) were purchased from commercial suppliers and housed in ~38 l aquaria illuminated with 100 W incandescent and UVB lights for 12 h per day. Lizards were provided with water *ad libitum* and fed crickets every day, except the day of experimentation. Experiments were conducted in accordance with the University of California, Riverside Animal Care and Use Protocol no. A-20140028.

Individuals were used in a succession of four procedures that were combined to create a comprehensive picture of the function of the gastrocnemius pars fibularis pars major (following Herrel et al., 2008a, and hereafter referred to as gastrocnemius for simplicity) in *A. equestris* (Fig. 1): (1) electromyography (EMG) experiments to obtain muscle activity data as animals ran on four different surfaces varying in incline and perch diameter, (2) *in situ* experiments to characterize force–length properties, (3) post-mortem manipulation of hindlimbs with muscles exposed to quantify the relationship between joint angle and muscle length, and (4) dissection and morphometric analysis of the muscles and tendons of the hindlimb to calculate maximum potential for tendon strain during cyclical locomotion in these animals.

EMG experiments

As described previously (Higham and Jayne, 2004; Foster and Higham, 2014), *A. equestris* were anaesthetized with an intramuscular injection of ketamine (100 mg kg^{-1}) into the left hindlimb prior to percutaneous implantation of a bipolar 0.051 mm diameter polycoated stainless-steel EMG electrode (California Fine Wire Co., Grover Beach, CA, USA) into the mid-belly of the right gastrocnemius. Following surgery, an intramuscular injection of the analgesic flunixin (1 mg kg^{-1}) was given. Dots were placed on the centre of each hindlimb joint to facilitate digitizing. Animals were allowed to recover from anaesthesia for 18–24 h.

Animals ran along four different 1 m-long trackways, each representing a combination of incline (0 or 30 deg) and perch diameter (a broad 30 cm-wide flat perch or a narrow 5 cm-diameter

perch). Trials were considered for analysis if the animals ran steadily and if the body remained on the dorsal surface of the perch. The trackways were covered in cork shelf liner to facilitate traction (Schmidt and Fischer, 2010; Foster and Higham, 2012, 2014). Two high-speed cameras (Phantom Miro M150, Vision Research Inc., Wayne, NJ, USA), operating at 1000 frames s^{-1}, were used to obtain dorsal and lateral video of the animals while simultaneously recording EMG data at 5000 samples s^{-1} using a BIOPAC MP150 data acquisition system with the UIM100C module and AcqKnowledge (v. 4.0) software (BIOPAC Systems, Inc., Goleta, CA, USA). Video and EMG recordings were synchronized using an external trigger. EMG signals were amplified 10,000 times and filtered with a 60 Hz notch filter using a Grass QU511 quad amplifier (Natus Neurology Inc., Warwick, RI, USA).

All EMG analyses followed Foster and Higham (2014). Briefly, EMG signals were rectified and filtered using low (70 Hz) and high (2500 Hz) bandpass filters prior to calculating burst onset and offset time, burst duration, magnitude and timing of peak burst amplitude, total rectified integrated area (RIA) during stance phase, and the time at which half of the burst RIA was achieved. To facilitate the averaging of data across strides and trials as well as subsequent calculations incorporating kinematic data, EMG amplitudes were divided into 40 bins for activity occurring during stance phase and 20 bins for swing phase activity (e.g. Fig. 1B), as in Foster and Higham (2014). All amplitudes were expressed relative to the maximum amplitude ever observed for each individual. Calculations were performed using custom code written for MATLAB (R2012a, The MathWorks, Natick, MA, USA) by K.L.F.

3D coordinates for each joint of the hindlimb were obtained using DLTdv5 (Hedrick, 2008) for MATLAB and then used to calculate body speed and magnitudes and velocities of femur depression, retraction and rotation, and knee and ankle angles using custom MATLAB code (Birn-Jeffery and Higham, 2014). Calculations followed Foster and Higham (2012). Trajectories of joint kinematics were binned as described for the EMG analyses (e.g. Fig. 1C) in order to compare across trials and individuals.

In situ force–length experiments

Following the EMG experiments, individuals were anaesthetized with an intramuscular injection of ketamine (300 mg kg^{-1}) and monitored to ensure continued, deep anaesthesia throughout experimentation.

An incision was made on the ventral surface of the femoral segment of the right hindlimb to isolate the sciatic nerve proximal to its first branching point. Although not prominent, any connective tissue surrounding the nerve was removed to ensure maximal contact between the nerve and electrode. A bipolar platinum hook electrode was then hooked around the nerve and mineral oil was applied to help maintain hydration of the nerve and minimize voltage dissipation during stimulation (Fig. 1F; Nelson et al., 2004). Mineral oil was reapplied at several points during experimentation to ensure consistent signal transmission. The other end of the hook electrode was attached to a Grass S48 Stimulator (Natus Neurology Inc.).

Next, the gastrocnemius muscle was carefully isolated. To anchor the proximal end of the gastrocnemius, the femur was held in place using machine screws built into the *in situ* apparatus and the distal end of the gastrocnemius was fastened to a servomotor (Aurora 300C, Aurora Scientific Inc., Aurora, ON, Canada) via a short (approximately 1 cm long) piece of silk suture tied around the proximal end of the gastrocnemius tendon. Because the tendon of the gastrocnemius is very short and slender in this species, a number of measures were taken to ensure that the suture could not slide during
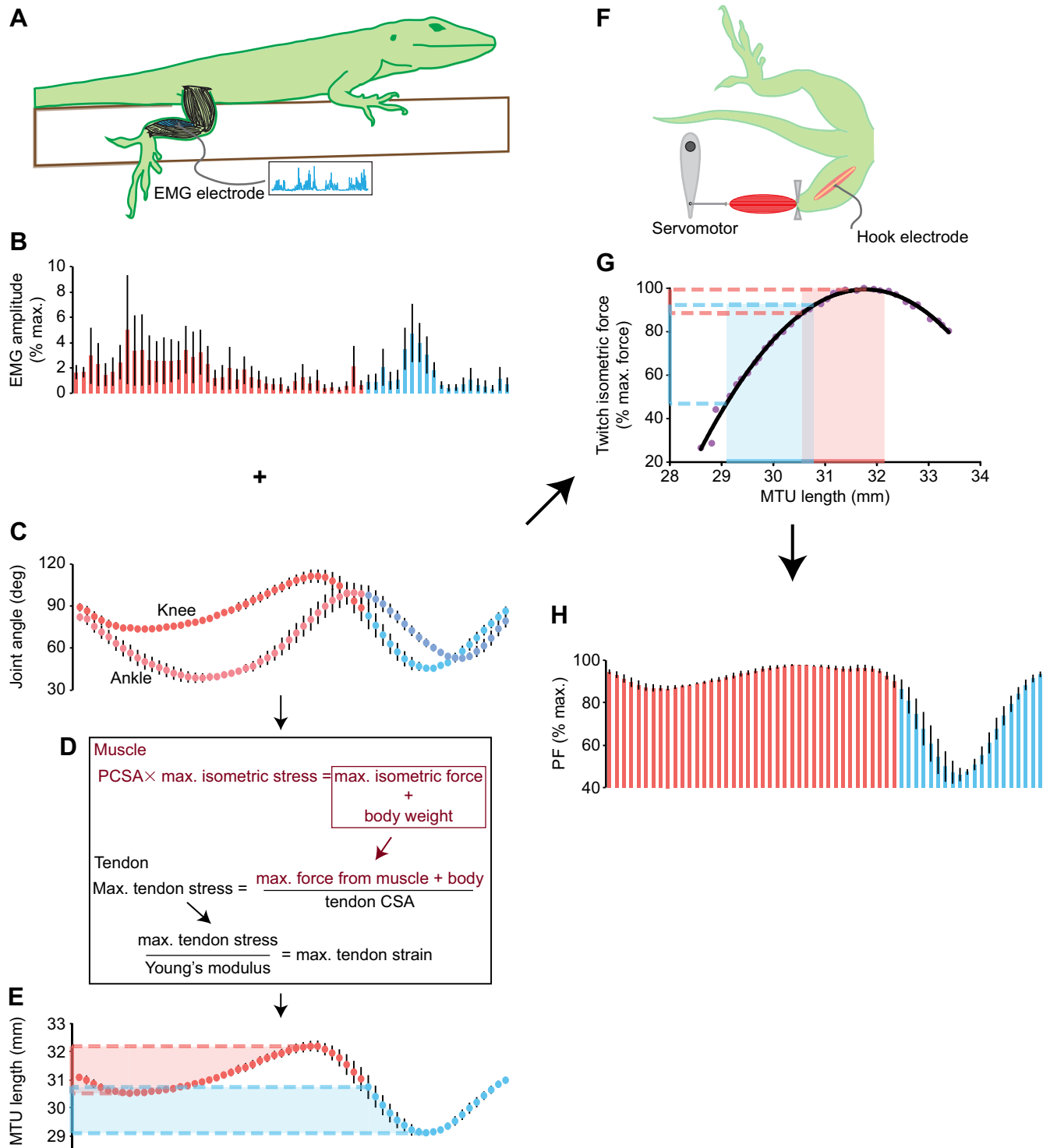
Fig. 1. Schematic illustration of the methodology employed in this study, with example mean data from a representative *Anolis equestris* individual running on the horizontal, broad perch. EMG data were collected for the gastrocnemius (A,B) as the animal was filmed with high-speed video to obtain 3D joint angles (C). Calculations (D) based on dissections and confirmed with *in situ* experiments demonstrated that tendons were unlikely to stretch during running, enabling calculation of muscle–tendon unit (MTU) length from joint angles and muscle morphology data (E). *In situ* stimulation of the sciatic nerve enabled construction of a twitch force–length curve (FLC) for the gastrocnemius (F,G). Using this curve, MTU lengths during stance phase (red) and swing phase (blue) could be used to calculate the corresponding potential isometric force (H). Max., maximum; CSA, cross-sectional area; PCSA, physiological CSA; PF, potential force. Values are means±s.e.m.

experimentation (verified with high-speed video). The majority of the crus, along with all other distal limb muscles, was removed by severing the limb just above the ankle and just below the knee after a piece of suture was tied below the knee as a tourniquet to reduce blood loss. Further, the weight at the distal end was minimized by removing all the toes of the foot. This arrangement meant that the ankle joint could be used as an anchor, past which the suture fastened to the distal gastrocnemius could not slide. This also ensured that no other muscles could contract and interfere with the gastrocnemius during sciatic nerve stimulation. A small drop of contact cement was placed on the knot tied around the tendon to prevent the knot from loosening.

Because the gastrocnemius of this species was too small for sonomicrometry, the length of the muscle prior to each stimulation event was measured using digital calipers (error±0.005 mm) and the length during contraction was monitored using the Aurora dual-mode lever system. All force and length signals from the Aurora lever system were sent to the same data acquisition system and software used for EMG experiments.

Before constructing an FLC for the gastrocnemius, the voltage at which we observed maximum force was determined by measuring the force generated during a twitch contraction when the sciatic nerve was stimulated at a series of voltages, beginning at 1 V and increasing in increments of 0.5 V. Once no further increase in twitch force was observed, the stimulation voltage was increased by 1 V to ensure supramaximal stimulation, which was used for all subsequent twitch and tetanic contractions.

To construct the twitch FLC, a single 0.2 ms pulse at the supramaximal stimulation voltage was sent to the sciatic nerve at each muscle length and the resulting force was recorded (Fig. 2). For the four individuals for which we obtained a tetanic FLC, the nerve was stimulated for 500 ms at a stimulation rate sufficient to allow good summation of the 0.2 ms pulses (0.01 ms delay between pulses) into a tetanic contraction. This stimulation rate varied between individuals, but ranged between 17 and 26 pulses s^{-1}. As tetanic contractions can result in muscle fatigue, 5 min of rest were provided between each successive stimulation event. In all cases, twitch FLCs were constructed prior to tetanic FLCs.

Calculation of maximum tendon strain

As the muscle was too small for sonomicrometry, we relied on the combination of instantaneous joint angles from our kinematic data
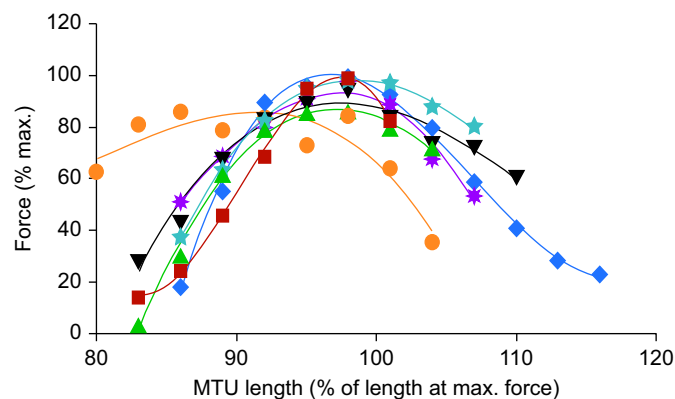

Fig. 2. Twitch FLCs for the gastrocnemius of *A. equestris* individuals. To facilitate visual comparison between individual FLCs, we reduced the number of points on each curve by binning data. Bins had a width of 3% of muscle length, and forces contained in each of those bins were averaged to create a single point per bin. This binning method did not alter the shape of the FLCs. Each symbol/colour represents a different individual, *n*=7.

and detailed morphology [i.e. muscle–tendon unit (MTU) length and moment arm] to estimate instantaneous muscle length *in vivo*. However, because changes in the length of the MTU can be caused by changes in the length of the muscle, the tendon, or a combination of the two (Higham and Nelson, 2008), it was necessary to first establish whether the tendon could be stretching during normal, cyclical locomotion in these animals. This was done using both morphometric data and *in situ* experimentation.

To calculate maximum tendon strain, in which positive values indicate lengthening, we measured mass, fascicle length, whole-muscle length, pennation angle, and origin and insertion point of each muscle of the proximal hindlimb and crus, as well as the mass and length of the associated tendons (Tables S1 and S2). These measurements were used to calculate maximum tendon strain (Fig. 1D). Briefly, we calculated the maximum force each hindlimb muscle could generate by multiplying physiological cross-sectional area by maximum isometric stress for vertebrate muscle (0.3 MPa; Wells, 1965; Medler, 2002). Next, we added body weight (body mass×gravitational acceleration) to this muscle force to simulate a scenario in which the focal muscle is responsible for propelling the entire body. Thus, this overestimated the maximum amount of force the focal tendon could experience during cyclical locomotion. We divided this force by tendon cross-sectional area to determine maximum tendon stress. Finally, although there is some debate about how elastic properties vary among vertebrates (Bennett et al., 1986; Pollock and Shadwick, 1994b; Matson et al., 2012), we divided tendon stress by an elastic modulus of 1.5 GPa (Bennett et al., 1986), which is within the range of values reported by these papers, to calculate maximum tendon strain.

To confirm calculations of maximum tendon strain, high-speed video was obtained for two individuals during maximal tetanic *in situ* contractions similar to those described above. After both twitch and tetanic FLCs had been obtained, the suture tied around the proximal end of the gastrocnemius tendon was removed and retied around the distal-most end of the tendon, just proximal to the insertion point on the pes. No damage to the tendon was visible. Two points were marked along a single muscle fascicle to help visualize any contraction of the muscle fibres that may be allowed through stretching of the tendon. Even though the entire MTU length was held constant by the experimental setup, tendon or aponeurosis stretching may permit the length of individual muscle fibres to decrease, resulting in a decrease in the distance between the points marked on the muscle fascicle. As the gastrocnemius of this species had no visible aponeurosis, we had no reason to expect a decoupling of muscle fibre length from MTU length without a corresponding change in tendon length. Thus, we assumed that all fascicles in the muscle belly were behaving in a similar manner to the marked fascicle and used the absence of a visible change in the distance between marked points to indicate an absence of muscle fibre and tendon length change.

Both the calculations and *in situ* experiments revealed that the gastrocnemius tendon is incapable of deforming significantly during normal cyclical locomotion in these animals (see Results).

Calculation of *in vivo* muscle length

Given that the gastrocnemius tendon was not capable of changing length, we generated a calibration curve to convert instantaneous joint angles into muscle lengths. To do this, the skin was removed from the left hindlimb and the thin connective tissue linking the gastrocnemius to other muscles of the crus was severed along the entire length of the muscle and tendon. This allowed the gastrocnemius to stretch and slide easily relative to the other

muscles in the limb as the knee and ankle were manipulated. The knee and ankle joints and origin and insertion points of the gastrocnemius muscle and tendon were painted with black nail polish to facilitate visualization in videos. The limb was manipulated with forceps through the entire 3D range of hip, knee and ankle angles normally observed during running in these animals. These manipulations were recorded with two high-speed video cameras and the resulting video was digitized as described for the EMG analyses above. MTU length was calculated using a combination of the 3D coordinates of the joints and the muscle and tendon landmarks. Estimation of *in vivo* muscle length from kinematics can be fraught with errors because of the ability of

skeletal structures to move relative to the skin (especially in mammals) and the potential for tendon strain to cause a decoupling between muscle length and MTU length. However, lizard skin is securely anchored to the underlying skeletal structures at the joints (K.L.F., personal observation), reducing the potential for error in our calculations of muscle length to approximately the level that is seen in any kinematic study of lizard locomotion.

Because the gastrocnemius is biarticular, crossing both the knee and ankle joints, a multiple regression was used to obtain the calibration curve that converted the instantaneous knee and ankle joints from the video of the EMG trials into instantaneous muscle lengths (Fig. 1E; custom MATLAB code written by K.L.F.). To
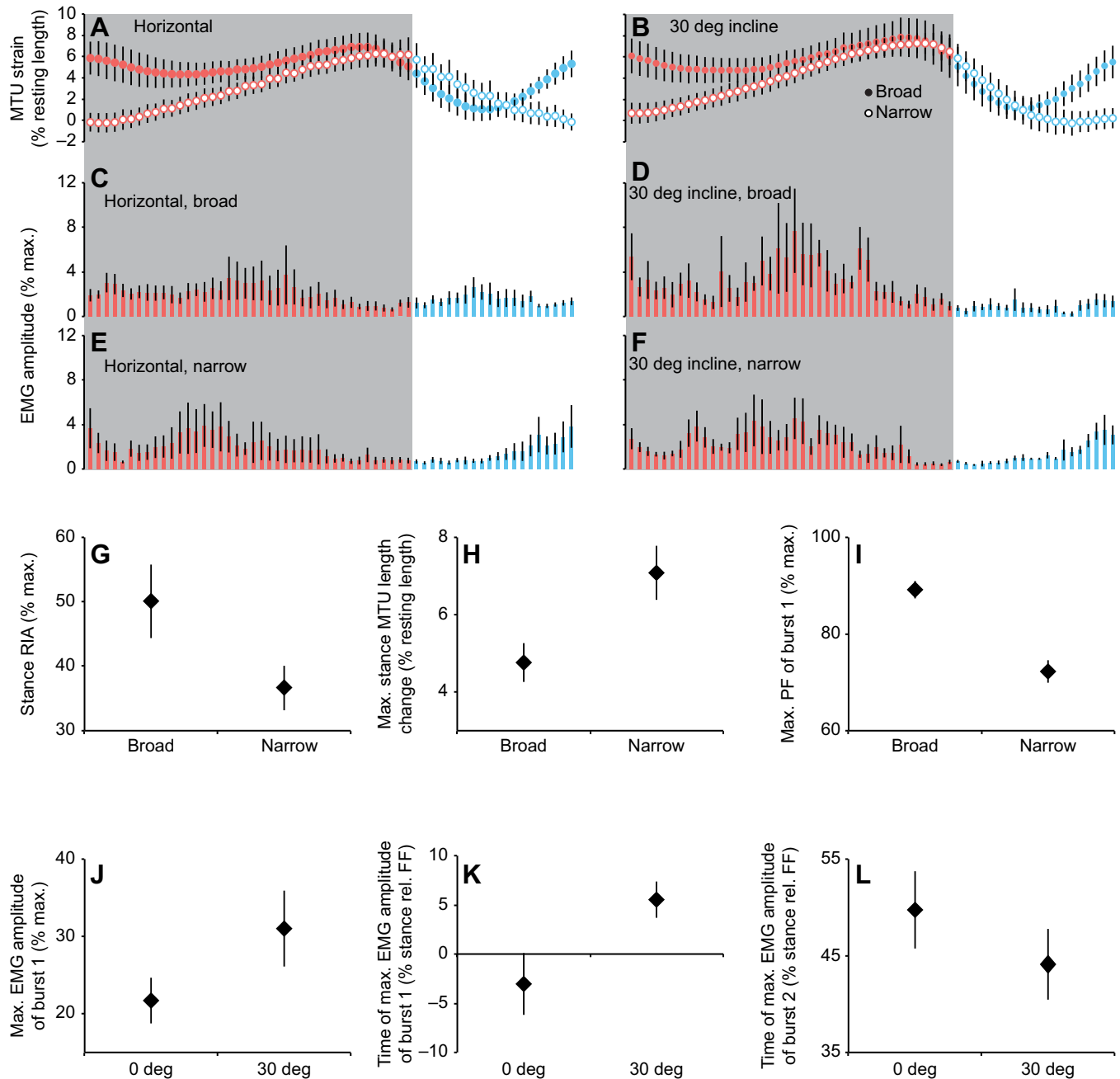
Fig. 3. The impact of perch diameter and incline on muscle strain and activation patterns. Binned MTU length trajectories (A,B), binned EMG amplitude (C–F), and significant relationships on perches of different diameter (G–I) and incline (J–L). In A–F, filled symbols indicate a broad perch, open symbols indicate a narrow perch; the shaded region (red data) is the stance phase, the unshaded region (blue data) is the swing phase. RIA, rectified integrated area; rel. FF, relative to footfall; PF, potential force. Values are means±s.e.m., *n*=6.

facilitate visual comparison of EMG amplitudes and instantaneous muscle lengths, we generated binned trajectories of muscle strain as described above (Fig. 3A,B). These muscle strain values were expressed as a percentage of resting muscle length, which was defined as the length of the muscle when the limb was positioned with knee and ankle angles at 90 deg.

Calculation of potential force

We defined potential force (PF) as the force that the gastrocnemius muscle could theoretically generate under isometric conditions as defined by the twitch FLC. Although the muscle is most certainly active for more than the duration of a single twitch, and thus is capable of generating greater total forces, the purpose of PF was not to calculate exact forces produced by the animals *in vivo*, but to determine the relative potential to generate force in the different conditions, with stimulation frequency and duration being equal. Further, although we generated tetanic FLCs as well, we viewed the twitch curves as being more biologically relevant as tetanic contractions are not observed in these animals during locomotion. We used the third-order polynomial that fitted the twitch FLC of each individual to calculate the PF that corresponded to any given MTU length for that individual. This process is illustrated in Fig. 1G, which shows the range of MTU lengths and corresponding PFs. These forces were then used to generate a trajectory of PFs through time (Fig. 1H). Finally, we used the onset and offset times of EMG bursts to determine the portions of the twitch FLC that corresponded to periods of activity of the muscle (i.e. the active portion of the FLC). From these regions, we identified the minimum and maximum PFs within each burst, as well as the minimum and maximum PFs generated during both periods of activity.

It is important to note that this PF calculation is highly dependent on the position of the FLC. Both the magnitude of the forces produced and the length at which maximum force production occurs on a given curve depend on the stimulation regime of the muscle. Not only do tetanic contractions achieve greater forces than twitch contractions but also increases in stimulation frequency and intensity result in an increased optimum length in tetanic FLCs in some vertebrates (Rack and Westbury, 1969; Holt and Azizi, 2014, 2016). Similarly, twitch curves can have considerably longer (∼40%) optimum lengths than tetanic curves (Holt and Azizi, 2014, 2016), although this is not always the case (Rack and Westbury,

1969). As seen in several cats in the study by Rack and Westbury (1969), there was virtually no shift in the horizontal position of the twitch and tetanic FLCs for the gastrocnemius muscles of our lizards (∼5% of tetanic optimum length). This fact, coupled with the biological relevance of twitch compared with tetanic contractions, led us to use the twitch FLCs for all PF calculations.

Statistical analyses

Prior to all analyses, the role of speed (SVL s^{-1}) was assessed by regressing it against all kinematic, EMG and force variables. We used the residuals of those variables that were significantly ($r>0.15$, $P<0.01$) impacted by speed. Principal component and discriminant function analyses used to analyse the kinematic data were performed in JMP (version 11, SAS Institute Inc., Cary, NC, USA). All other analyses (i.e. mixed-model analyses of variance, ANOVA) were performed with SYSTAT (version 13, Systat Software, Inc., San Jose, CA, USA).

As described previously (Foster and Higham, 2012), kinematic variables were separated into temporal (angular velocities, stride frequency, duty factor) and angular (magnitudes of joint angles observed at the beginning, middle and end of stance, as well as minimum, maximum and excursion of angles) variables before being inserted into a principal components analysis (PCA) to reduce dimensionality and identify the 12 variables most important for generating the majority of the variation between treatments. The number of variables chosen from each of the first two PC axes corresponded to the proportion of variance explained by those axes (Foster and Higham, 2012). These variables were then loaded into a discriminant function analysis (DFA; Fig. 4) and variables that loaded heavily (greater than ±0.3) on a significant axis were considered significant for explaining kinematic differences between treatments (Tables S3 and S4). Finally, *post hoc* one-way ANOVA were performed on DFA scores to determine which treatments were significantly different from each other.

Force and EMG data were analysed using mixed-model ANOVA in which individual was a random factor and perch diameter and incline were fixed factors (Foster and Higham, 2014). To obtain the correct *F*-values for incline and perch diameter in this design, the mean squares for each of these factors were divided by the mean squares of the interaction between individual and each fixed factor, and the corrected denominator for the degrees of freedom was the degrees of freedom of this interaction (Zar, 1999).
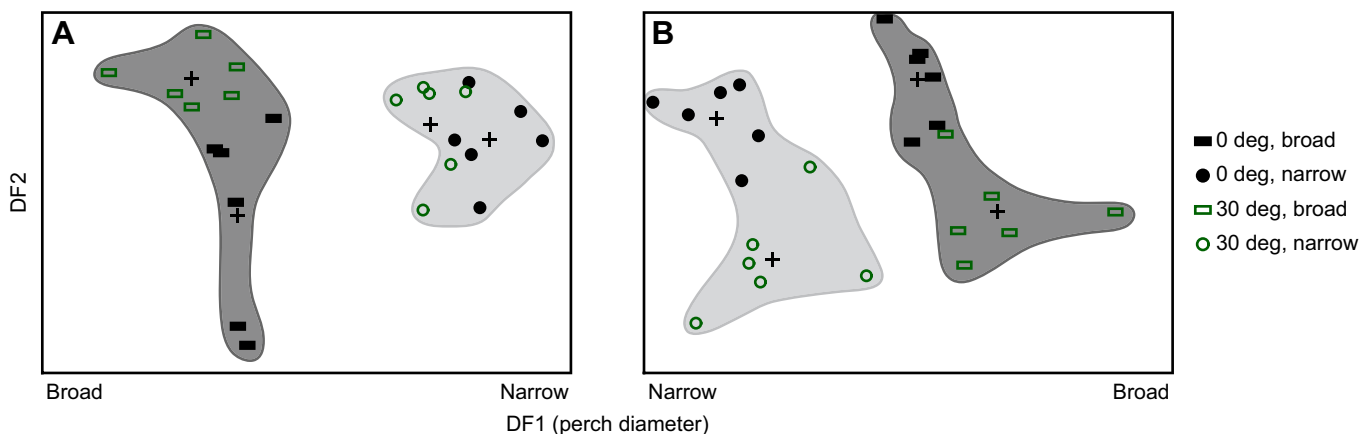
Fig. 4. First two axes of discriminant function (DF) analyses of hindlimb joint angles and angular velocities of *A. equestris*. (A) Hindlimb joint angle; (B) angular velocity (*n*=6). The mean for each treatment is indicated by a cross. Filled symbols, horizontal treatment; open symbols, 30 deg incline; rectangles, broad perch; circles, narrow perch. Regions occupied by broad and narrow treatments are shaded in dark and light grey, respectively. DF2 was not significant in either DF analysis. *P*-values and canonical loadings on each axis are given in Tables S3 and S4.

RESULTS

Changes in kinematics with perch diameter and incline

For both angular and velocity DFAs, only the first discriminant axis, which described perch diameter, was significant (Fig. 4; Tables S3 and S4). Therefore, all significant changes in kinematics described here are associated with changes in perch diameter.

The majority of the angular variables affected by changes in perch diameter were associated with the proximal joints (Table S3). The pelvic girdle was less rotated and the femur was more depressed on the narrow perch than on the broad perch (Table S5). The femur rotated less and achieved its maximum long-axis rotation later in swing phase on the narrow perch than on the broad perch (Table S5). Further, maximum knee flexion occurred earlier in stance phase on the narrow perch than on the broad perch (Table S5).

Changes in joint angular velocities with perch diameter were generally associated with the distal joints (Table S4). During stance phase, both the knee and the ankle extended faster on the narrow perch than on the broad perch (Table S5). The average angular velocity of the knee during swing phase indicated that it was generally extending (positive angular velocity) during recovery on the broad perch but flexing (negative angular velocity) during recovery on the narrow perch (Table S5). Also, during swing phase, both ankle extension and femur long-axis rotation [in the counter-clockwise (i.e. negative) direction] occurred slower on the narrow perch than on the broad perch (Table S5).

Tendon function during cyclical locomotion

The most any hindlimb tendon could stretch during non-ballistic, cyclical locomotion in *A. equestris* is 0.191 mm, or 0.863% of MTU length in the tendon of the ilioishiofibularis (Table S2). In contrast, the tendon of the gastrocnemius, the focal muscle in this study, could stretch only 0.037% of MTU length (Table S2), which reflects a maximum strain energy storage of 0.000239 J kg^{-1} body mass. This is several orders of magnitude lower than the strain energy storage seen in the Tamar wallaby (0.1325 J kg^{-1} body mass; Biewener and Baudinette, 1995), which is known for using elastic energy storage for hopping. Further, for *in situ* experiments performed under conditions of maximal tetanic stimulation, high-speed video of a marked muscle fascicle revealed no change in muscle fibre length or tendon length. Thus, neither the tendon of the gastrocnemius nor

any other hindlimb tendon is capable of deforming during cyclical locomotion in *A. equestris*.

Changes in gastrocnemius muscle function with perch diameter and incline

The gastrocnemius exhibited two bursts per stride, the first centred on footfall and the second occurring in mid- to late stance (Fig. 5B). Muscle length was fairly constant during the propulsive portion of stance, with values of strain ranging from 4.77±0.5% on broad surfaces to 7.10±0.70% on narrow surfaces. Further, gastrocnemius activity always occurred on the ascending and plateau regions of the FLC (Fig. 1G).

Shifts in the operating length and PF generated by the gastrocnemius occurred only for perch diameter. Total RIA during stance was lower on the narrow perch (36.62±3.45% maximum amplitude) than on the broad surface (50.11±5.74% maximum amplitude, P=0.039; Fig. 3G). Further, the maximum range of MTU operating lengths was larger on the narrow perch (7.10±0.70%) than on the broad perch (4.77±0.5%, P=0.019; Fig. 3H), primarily due to lower values of strain at the beginning of stance on the narrow perch compared with the broad perch (Fig. 3A,B). Finally, both the minimum and maximum PF (Fig. 3I) during burst 1 were lower (minimum P=0.030; maximum P=0.016) on the narrow surface (minimum PF=52.70±4.08% maximum force; maximum PF=72.27±2.37% maximum force) compared with the broad surface (minimum PF=72.44±2.52% maximum force; maximum PF=89.13±1.77% maximum force).

On the steeper incline, the maximum EMG amplitude of burst 1 was greater (31.02±4.92% maximum amplitude) than on the horizontal surface (21.68±2.99% maximum amplitude, P=0.020; Fig. 3J). Further, this occurred later for the 30 deg treatment (5.53±1.86% from beginning of stride) than for the horizontal treatment (3.03±3.14% before beginning of stride, P=0.041; Fig. 3K). In contrast, the time of peak burst 2 amplitude occurred earlier in stance phase on the 30 deg incline (44.11±3.68% from beginning of stride) than on the horizontal surface (49.75±4.02% from beginning of stride, P=0.043; Fig. 3L). Although changes in incline did not appear to elicit shifts in either operating length or PF, incline significantly impacted the relationship between PF and muscle recruitment during stance (t=2.20, d.f.=20, P=0.04; Fig. 6). On horizontal treatments there was a negative relationship
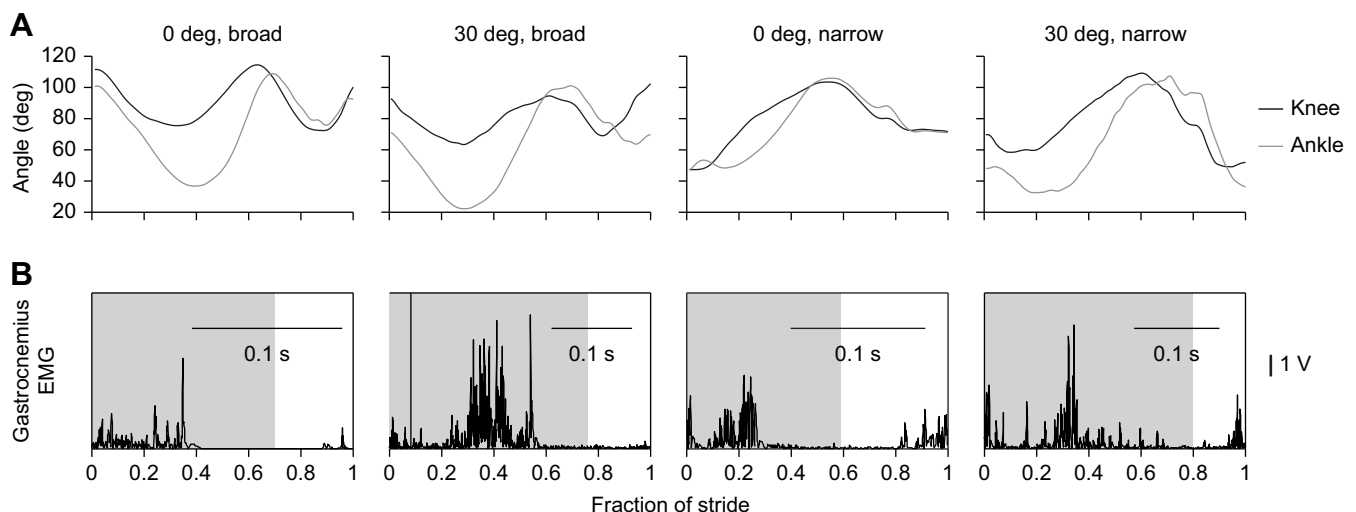

Fig. 5. Joint angles and muscle activity patterns for a single representative stride in each condition. (A) Knee and ankle angles; (B) gastrocnemius EMG trace. The shaded area represents stance phase.
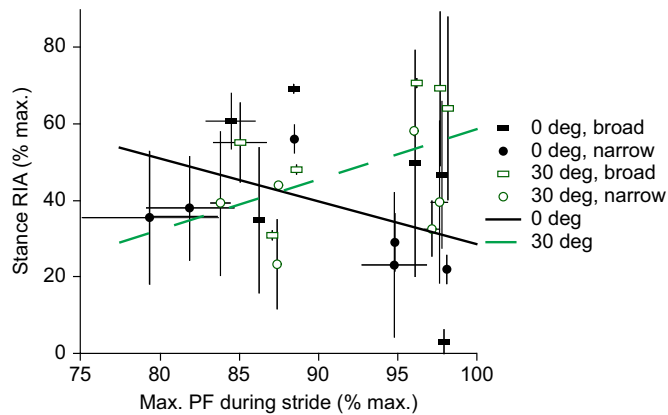
Fig. 6. Regressions of RIA during stance phase versus maximum PF during any period of muscle activity during the stride. Data are for the horizontal surface (solid black line) and 30 deg incline (green dashed line). The slopes of the regressions were significantly different (P=0.04). Symbols represent means for each individual for each treatment condition (n=6). Standard error bars represent variation between strides for each individual for that condition. Filled symbols, horizontal treatment; open symbols, 30 deg incline; rectangles, broad perch; circles, narrow perch.

between PF and stance RIA (slope=−1.12, r^2=0.16) whereas on the inclined surfaces this relationship was positive (slope=1.32, r^2=0.23).

DISCUSSION

By combining *in vivo* and *in situ* techniques with gross morphological dissection, we gained a comprehensive understanding of gastrocnemius function in response to both incline and perch diameter in an arboreal lizard (*A. equestris*). Not only were kinematics more strongly affected by alterations in perch diameter than incline but also both the level of effort (i.e. muscle recruitment) and the efficacy of force generation (i.e. PF) were greater on the broad surface, where ankle extension has greater opportunity to contribute to propulsion, than on the narrow surface. Therefore, it appears that the gastrocnemius may be actively and anatomically tuned to function most effectively on broad perches. Furthermore, increasing incline not only resulted in familiar shifts in the magnitude and timing of muscle activity to increase the muscle recruitment during the propulsive phase of the stride (Carlson-Kuhta et al., 1998; Gillis and Biewener, 2002; Daley and Biewener, 2003; Higham and Jayne, 2004; Foster and Higham, 2014) but also altered the relationship between force-generating capacity and muscle recruitment. On horizontal surfaces, where the gastrocnemius was operating over more optimal portions of the FLC and was theoretically capable of generating greater forces, there was a corresponding drop in muscle recruitment. However, on inclined surfaces, there was a positive relationship between PF and muscle recruitment. Thus, it appears that demands imposed by the physical environment have the potential to impact fundamental principles governing the interaction between behavioural and physiological aspects of muscle function.

Perch diameter greatly alters kinematics and muscle function

As in other studies, the majority of the compensatory shifts in limb kinematics on different perch diameters occurred in the proximal rather than the distal joints (Spezzano and Jayne, 2004; Foster and Higham, 2012, 2014). Differences in the geometry of the two perch surfaces explain the vast majority of the angular and angular velocity

changes observed here. On the narrow perch, *A. equestris* places its hindlimbs on the sides of the perch. With the pes in this location, propulsion is characterized by rapid extension of the knee and ankle before the pes abducts and falls away from the sides of the perch to begin swing phase. This contrasts with the broad perch, where the entire foot, including digits, is in an orientation that allows knee and ankle extension to contribute significantly to forward propulsion, as is well recognized in terrestrial animals (Brinkman, 1980; Gregersen et al., 1998; Russell and Bels, 2001; McGowan et al., 2005, 2008; Arnold et al., 2013).

The greater reliance on ankle extension for propulsion on the broad surface may explain the shifts in gastrocnemius with changes in perch diameter. Stance RIA was greater on the broad surface than on the narrow surface, indicating that the muscle was working 'harder'. Further, PF was greater and MTU strain was lower during the stance phase on the broad compared with the narrow surface. This suggests that the gastrocnemius was functioning more effectively by operating on a more optimal region of its FLC on the broader perch compared with the narrow perch. The gastrocnemius was, therefore, contributing more to propulsion on the broader surface.

Because the gastrocnemius may be less equipped to function effectively on narrow surfaces than on broad surfaces, other muscles may exhibit an increased propulsive effort on narrow perches in order to maintain a given level of locomotor performance, effectively altering how the locomotor system is functioning. The puboischiotibialis, a major limb depressor and knee flexor, is an obvious candidate for taking on a more influential role during locomotion on narrow surfaces (Higham and Jayne, 2004; Foster and Higham, 2014). Assuming an adaptive advantage to moving effectively on narrow surfaces, a reasonable assumption given that this animal lives primarily in the crowns of trees, we would expect that this muscle would be functioning closest to the plateau region of its FLC when the limb is more depressed as it is on narrow perches. Although beyond the scope of this study, examining how the roles of other muscles change to compensate for the shift in the propulsive contribution of the gastrocnemius is needed.

Incline affects the relationship between PF and muscle recruitment

We propose that a fundamental mechanism by which ecological challenges can impact muscle function involves affecting the relationship between 'how hard' muscles are working (i.e. muscle recruitment) and how effective they are at generating force (i.e. active location on the FLC). If these active lengths shift so that the force the muscle is capable of generating increases, one might consider it to be functioning more effectively (Roberts et al., 1997). Assuming no alteration in the demands placed on the animal, it is reasonable to expect that a muscle that is generating force more effectively would not need to recruit as many motor units to accomplish a given task as a muscle that is functioning on a suboptimal position on the FLC, resulting in a negative relationship between PF and muscle recruitment. This is analogous to the trade-off between muscle shortening velocity and motor unit recruitment (Roberts and Azizi, 2011). Alternatively, if there is an increase in the demand placed on the animal, muscle fibre recruitment may remain constant or even increase, despite generating forces more effectively in order to meet those increased demands. This would result in a positive relationship between PF and muscle recruitment. Interestingly, we saw both relationships. Regardless of perch diameter, animals whose gastrocnemius muscles were functioning at more optimal portions on the FLC decreased motor unit recruitment during the

stance phase on horizontal surfaces (negative relationship) but increased muscle fibre recruitment on 30 deg inclines (positive relationship; Fig. 6). Thus, it appears that the increased muscle work required on inclines (Cartmill, 1985; Preuschoft, 2002) disrupts the expected trade-off between PF and muscle recruitment observed on horizontal surfaces. Whether this pattern prevails in other vertebrate groups remains to be seen.

Tendons function to transfer force during locomotion of small lizards

We provide strong evidence that neither the tendon of the gastrocnemius nor any other hindlimb tendon is likely to stretch and store elastic energy during cyclical locomotor tasks in *A. equestris*. This is not surprising given that the combination of relatively constant tendon material properties (Bennett et al., 1986; Pollock and Shadwick, 1994b; but see Matson et al., 2012) and positive allometry of muscle cross-sectional area means that smaller animals are less likely to be able to generate the forces necessary to stretch their tendons (Biewener et al., 1981; Biewener and Blickhan, 1988; Pollock and Shadwick, 1994a). Although even a small deformation of the tendon could be biologically meaningful in small animals, as elastic energy storage represents a larger proportion of

the mechanical work of locomotion as body size decreases (Bullimore and Burn, 2005), it is possible that other structures (e.g. titin) could be more important for locomotor efficiency in this species (Nishikawa et al., 2012). Further investigation into the roles of these structures is critical for a thorough understanding of the energetics of *Anolis* locomotion.

The muscle forces we used in our calculations were estimated assuming maximal motor unit recruitment under isometric conditions, and the entire weight of the animal was added to those forces such that each muscle was theoretically independently responsible for supporting and propelling the body. Even though the elastic modulus of a tendon may not always be constant (Matson et al., 2012), the value used in our calculations fell within the range of those reported in the literature (Bennett et al., 1986; Pollock and Shadwick, 1994b; Matson et al., 2012); halving this value would still result in tendon strains well below 0.1% of MTU length. Further, our *in situ* experiments demonstrated that the gastrocnemius tendon would not deform even in the face of a supramaximal tetanic contraction, which is not likely to be biologically relevant. Therefore, we conclude that, excluding ballistic behaviours, hindlimb tendons are functioning to transmit force, rather than store elastic energy, in this species.
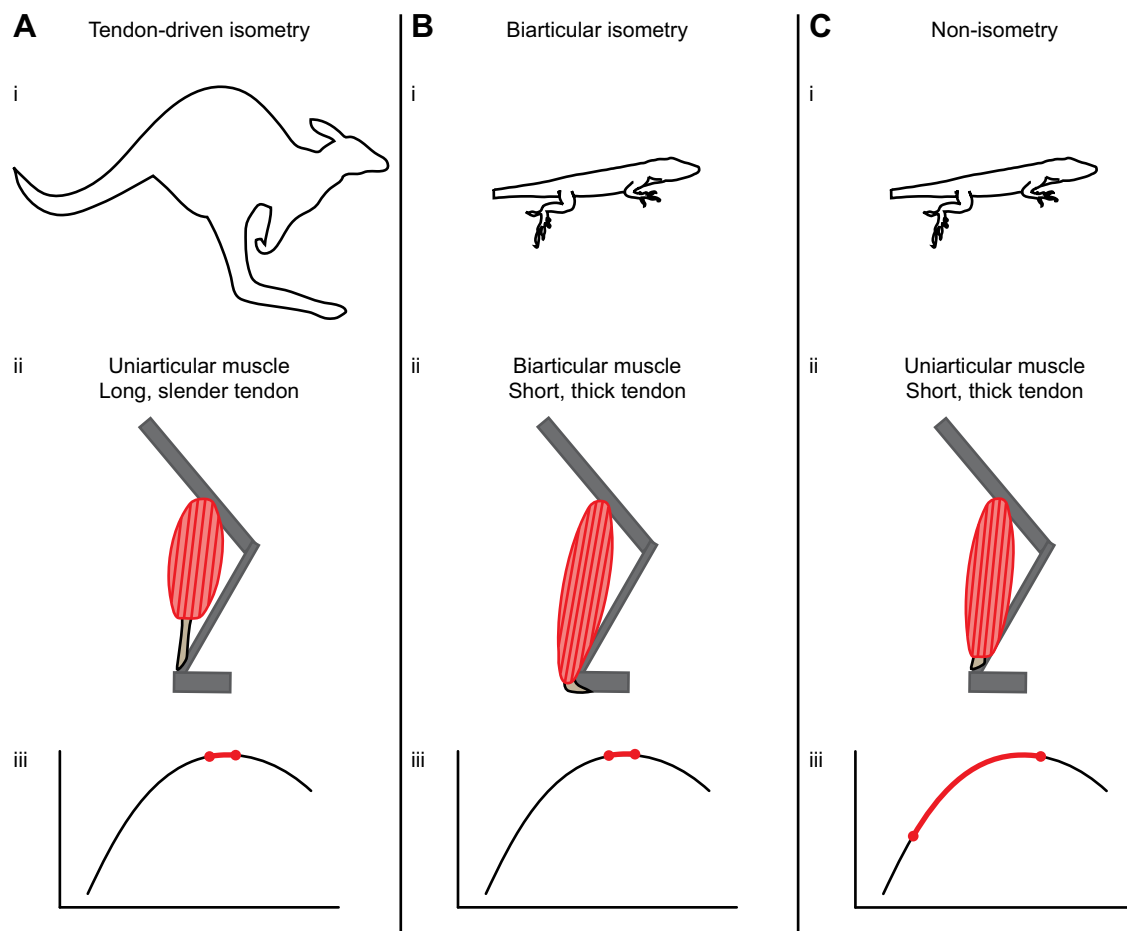
Fig. 7. Comparison of muscles contracting via tendon-driven isometry, biarticular isometry and non-isometry. Tendon-driven isometry (A) probably occurs primarily in larger animals (i) that have sufficient body mass to deform long, comparatively slender tendons (ii), allowing the muscle fibres to function over a very narrow range of lengths (i.e. isometrically) on the FLC (iii). Biarticular isometry (B) is likely to be the predominant mechanism of achieving isometry in small animals (i) that lack the body mass/muscle force to stretch shorter, comparatively thicker tendons (ii). However, as the muscle is biarticular, simultaneous extension and flexion in the two joints allows the muscle to function over a very narrow range of lengths on the FLC (iii). Non-isometric contractions (C) probably occur in uniarticular (ii) muscle of small animals (i) because changes in MTU length caused by joint flexion/extension translate directly into large changes in muscle length on the FLC (iii) as the tendon cannot stretch.

Most terrestrial vertebrates that have been the focus of *in vivo* muscle studies are necessarily amenable to invasive procedures and, concomitantly, are relatively large. Examples include turkeys (Roberts et al., 2007; Higham and Nelson, 2008), guinea fowl (Daley and Biewener, 2003; Higham and Biewener, 2008, 2011; Higham et al., 2008), wallabies (Biewener, 1998), horses (Wickler et al., 2005) and goats (McGuigan et al., 2009). Because of the skew towards larger animals, it is possible that our understanding of muscle function under *in vivo* conditions is also skewed. Some data do exist for smaller terrestrial vertebrates that have muscles large enough to use sonomicrometry to determine *in vivo* muscle lengths (e.g. Olson and Marsh, 1998; Holt and Azizi, 2016). However, in many small vertebrates, including *A. equestris*, the muscles are of insufficient size for sonomicrometry. Our approach to studying the dynamics of muscle function in small terrestrial animals, capitalizing on the fact that the kinematic and morphological data can be used to infer *in vivo* muscle lengths, will provide new insights and opportunities for comparisons across body sizes. Linking kinematics (i.e. curvature of the midline) with muscle lengths has proven useful for studying muscle function in swimming fishes (Katz and Shadwick, 1998; Shadwick et al., 1998; Donley and Shadwick, 2003), although this relationship becomes decoupled in lamnid/thunniform swimmers that have a different muscle/tendon arrangement (Donley et al., 2005; Shadwick and Syme, 2008).

Biarticularity facilitates isometric function during locomotion in *A. equestris*

The maximum gastrocnemius MTU strain observed during stance phase in *A. equestris* ranged from 4.77±0.5% on broad surfaces to 7.10±0.70% on narrow surfaces. These values are comparable to other experiments reporting isometric gastrocnemius contractions and fall well below length changes in other muscles and animals (Biewener, 1998; Gillis and Biewener, 2002; Wickler et al., 2005). Therefore, gastrocnemius MTU strain in *A. equestris* falls within the range expected for muscles that achieve economical force production (as opposed to high power) through isometric contraction. Interestingly, however, *A. equestris* appears to achieve this isometry via a different mechanism from that in other vertebrates.

There are at least two ways to achieve isometric force production when joint angles are changing: (1) MTU length may change as a result of changes in joint angles but the MTU length change may be caused solely by deformation of a series elastic element (e.g. tendon), allowing the muscle to maintain a constant length during force production (tendon-driven isometry), or (2) MTU length may remain relatively constant if the muscle is biarticular because coincident changes in angle of the two joints may counteract each other (biarticular isometry; Fig. 7A,B). A third less obvious scenario involves inter-muscular interactions across limb segments, such as the triarticular complex made up of the iliotibialis cranialis, iliotibialis lateralis pars preacetabularis and the medial gastrocnemius in guinea fowl (Higham and Biewener, 2011). The first two mechanisms of achieving isometry relate to two behavioural modes (cyclical versus ballistic locomotion) or two body sizes (small versus large; Fig. 7A,B). Large animals have sufficient mass and are capable of generating sufficient muscle forces to stretch their tendons during both behavioural modes and so can utilize tendon-driven isometry (Alexander, 1974; Alexander and Vernon, 1975; Biewener, 1998). In contrast, small animals that lack the body mass and muscle force capacity to stretch tendons (Biewener et al., 1981; Biewener and Blickhan, 1988; Pollock and Shadwick, 1994a) must rely on biarticular isometry when using a

cyclical locomotor mode because, unlike in ballistic movements, there is insufficient time to employ a catch mechanism (Astley and Roberts, 2012) to help load the tendon in advance (Fig. 7B). Therefore, as the gastrocnemius of *A. equestris* crosses both knee and ankle joints and the tendon of the gastrocnemius is unlikely to be deforming during running, it may be that biarticular isometry is the only mechanism by which it is able to achieve effective force production under conditions that require joints to move through large angular excursions. This may partially explain the presence of biarticular muscles in animals that need to move effectively under many different conditions. Biarticular muscles are common in vertebrates and it is tempting to propose that isometric force production may be one of the driving forces behind the evolution of such a morphological arrangement, but more research is needed.

Our study focused on inclines and different perch diameters, but it should be noted that, in nature, these animals are likely to be performing many additional behaviours (e.g. jumping, landing, turning) on substrates that also vary in many other aspects (e.g. texture, rugosity, compliance). Investigating how the gastrocnemius and other muscles contribute to performance in these ecologically relevant situations will be critical for discerning the relationships between physiology, biomechanics and ecology in *Anolis*.

Author contributions
K.L.F. and T.E.H. were involved in conceiving and designing the study, K.L.F. performed all experiments and data analyses and drafted the manuscript, and T.E.H. was involved in revising the manuscript. All authors gave final approval for publication.

Data availability
Data are available from the Dryad digital repository: doi:10.5061/dryad.2vt32 (Foster and Higham, 2017). Custom code can be obtained from the corresponding author upon request.

Supplementary information
Supplementary information available online at
http://jeb.biologists.org/lookup/doi/10.1242/jeb.151795.supplemental

References
Alexander, R. M. N. (1974). The mechanics of jumping by a dog (*Canis familiaris*). *J. Zool.* **173**, 549-573.
Alexander, R. M. N. and Vernon, A. (1975). The mechanics of hopping by kangaroos (Macropodidae). *J. Zool.* **177**, 265-303.
Arnold, A. S., Lee, D. V. and Biewener, A. A. (2013). Modulation of joint moments and work in the goat hindlimb with locomotor speed and surface grade. *J. Exp. Biol.* **216**, 2201-2212.
Astley, H. C. and Roberts, T. J. (2012). Evidence for a vertebrate catapult: elastic energy storage in the plantaris tendon during frog jumping. *Biol. Lett.* **8**, 386-389.
Bennett, M. B., Ker, R. F., Imery, N. J. and Alexander, R. M. N. (1986). Mechanical properties of various mammalian tendons. *J. Zool.* **209**, 537-548.
Biewener, A. A. (1998). Muscle function *in vivo*: a comparison of muscles used for elastic energy savings *versus* muscles used to generate mechanical power. *Amer. Zool.* **38**, 703-717.
Biewener, A. and Baudinette, R. (1995). *In vivo* muscle force and elastic energy storage during steady-speed hopping of tammar wallabies (*Macropus eugenii*). *J. Exp. Biol.* **198**, 1829-1841.
Biewener, A. A. and Blickhan, R. (1988). Kangaroo rat locomotion: design for elastic energy storage or acceleration? *J. Exp. Biol.* **140**, 243-255.

Biewener, A. A. and Gillis, G. B. (1999). Dynamics of muscle function during locomotion: accommodating variable conditions. *J. Exp. Biol.* **202**, 3387-3396.

Biewener, A., Alexander, R. M. N. and Heglund, N. C. (1981). Elastic energy storage in the hopping of kangaroo rats (*Dipodomys spectabilis*). *J. Zool.* **195**, 369-383.

Birn-Jeffery, A. V. and Higham, T. E. (2014). Geckos significantly alter foot orientation to facilitate adhesion during downhill locomotion. *Biol. Lett.* **10**, 20140456.

Brinkman, D. (1980). The hind limb step cycle of *Caiman sclerops* and the mechanics of the crocodile tarsus and metatarsus. *Can. J. Zool.* **58**, 2187-2200.

Bullimore, S. R. and Burn, J. F. (2005). Scaling of elastic energy storage in mammalian limb tendons: do small mammals really lose out? *Biol. Lett.* **1**, 57-59.

Carlson-Kuhta, P., Trank, T. V. and Smith, J. L. (1998). Forms of forward quadrupedal locomotion. II. A comparison of posture, hindlimb kinematics, and motor patterns for upslope and level walking. *J. Neurophysiol.* **79**, 1687-1701.

Cartmill, M. (1985). Climbing. In *Functional Vertebrate Morphology* (ed. M. Hildebrand, D. M. Bramble, K. F. Liem and D. B. Wake), pp. 73-88. Cambridge, MA: Harvard University Press.

Daley, M. A. and Biewener, A. A. (2003). Muscle force-length dynamics during level versus incline locomotion: a comparison of *in vivo* performance of two guinea fowl ankle extensors. *J. Exp. Biol.* **206**, 2941-2958.

Donley, J. M. and Shadwick, R. E. (2003). Steady swimming muscle dynamics in the leopard shark *Triakis semifasciata*. *J. Exp. Biol.* **206**, 1117-1126.

Donley, J. M., Shadwick, R. E., Sepulveda, C. A., Konstantinidis, P. and Gemballa, S. (2005). Patterns of red muscle strain/activation and body kinematics during steady swimming in a lamnid shark, the shortfin mako (*Isurus oxyrinchus*). *J. Exp. Biol.* **208**, 2377-2387.

Foster, K. L. and Higham, T. E. (2012). How forelimb and hindlimb function changes with incline and perch diameter in the green anole, *Anolis carolinensis*. *J. Exp. Biol.* **215**, 2288-2300.

Foster, K. L. and Higham, T. E. (2014). Context-dependent changes in motor control and kinematics during locomotion: modulation and decoupling. *Proc. R. Soc. B Biol. Sci.* **281**, 20133331.

Foster, K. L. and Higham, T. E. (2017). Data from: Integrating gastrocnemius force–length properties, *in vivo* activation and operating lengths reveals how *Anolis* deal with ecological challenges. *Dryad Digital Repository* doi:10.5061/dryad.2vt32.

Foster, K. L., Collins, C. E., Higham, T. E. Garland, T. J. (2015). Determinants of lizard escape performance: decision, motivation, ability, and opportunity. In *Escaping from Predators: An Integrative View of Escape Decisions and Refuge Use* (ed. W. E. Cooper, Jr and D. Blumstein), pp. 287-321. London: Cambridge University Press.

Gabaldón, A. M., Nelson, F. E. and Roberts, T. J. (2004). Mechanical function of two ankle extensors in wild turkeys: shifts from energy production to energy absorption during incline versus decline running. *J. Exp. Biol.* **207**, 2277-2288.

Gillis, G. B. and Biewener, A. A. (2002). Effects of surface grade on proximal hindlimb muscle strain and activation during rat locomotion. *J. Appl. Physiol.* **93**, 1731-1743.

Gregersen, C. S., Silverton, N. A. and Carrier, D. R. (1998). External work and potential for elastic storage at the limb joints of running dogs. *J. Exp. Biol.* **201**, 3197-3210.

Hedrick, T. L. (2008). Software techniques for two- and three-dimensional kinematic measurements of biological and biomimetic systems. *Bioinspir. Biomim.* **3**, 034001.

Herrel, A., Vanhooydonck, B., Porck, J. and Irschick, D. J. (2008a). Anatomical basis of differences in locomotor behavior in *Anolis* lizards: a comparison between two ecomorphs. *Bull. Mus. Comp. Zool.* **159**, 213-238.

Herrel, A., Schaerlaeken, V., Ross, C., Meyers, J., Nishikawa, K., Abdala, V., Manzano, A. and Aerts, P. (2008b). Electromyography and the evolution of motor control: limitations and insights. *Integr. Comp. Biol.* **48**, 261-271.

Higham, T. E. and Biewener, A. A. (2008). Integration within and between muscles during terrestrial locomotion: effects of incline and speed. *J. Exp. Biol.* **211**, 2303-2316.

Higham, T. E. and Biewener, A. A. (2011). Functional and architectural complexity within and between muscles: regional variation and intermuscular force transmission. *Philos. Trans. R. Soc. Lond. B. Biol. Sci.* **366**, 1477-1487.

Higham, T. E. and Jayne, B. C. (2004). *In vivo* muscle activity in the hindlimb of the arboreal lizard, *Chamaeleo calyptratus*: general patterns and the effects of incline. *J. Exp. Biol.* **207**, 249-261.

Higham, T. E. and Nelson, F. E. (2008). The integration of lateral gastrocnemius muscle function and kinematics in running turkeys. *Zoology* **111**, 483-493.

Higham, T. E., Biewener, A. A. and Wakeling, J. M. (2008). Functional diversification within and between muscle synergists during locomotion. *Biol. Lett.* **4**, 41-44.

Holt, N. C. and Azizi, E. (2014). What drives activation-dependent shifts in the force–length curve? *Biol. Lett.* **10**, 201400651.

Holt, N. C. and Azizi, E. (2016). The effect of activation level on muscle function during locomotion: are optimal lengths and velocities always used? *Proc. R. Soc. B Biol. Sci.* **283**, 20152832.

Irschick, D. J. and Higham, T. E. (2016). *Animal Athletes: An Ecological and Evolutionary Approach*. New York: Oxford University Press.

Johnston, I. A. (1991). Muscle action during locomotion: a comparative perspective. *J. Exp. Biol.* **160**, 167-185.

Katz, S. L. and Shadwick, R. E. (1998). Curvature of swimming fish midlines as an index of muscle strain suggests swimming muscle produces net positive work. *J. Theor. Biol.* **193**, 243-256.

Loeb, G. E. and Gans, C. (1986). The organization of muscle. In *Electromyography for Experimentalists*, pp. 25-43. Chicago: University of Chicago Press.

Losos, J. B. (1994). Integrative approaches to evolutionary ecology: *Anolis* lizards as model systems. *Annu. Rev. Ecol. Syst.* **25**, 467-493.

Losos, J. B. (2009). *Lizards in an Evolutionary Tree: Ecology and Adaptive Radiation of Anoles*. Berkeley, CA: University of California Press.

Matson, A., Konow, N., Miller, S., Konow, P. P. and Roberts, T. J. (2012). Tendon material properties vary and are interdependent among turkey hindlimb muscles. *J. Exp. Biol.* **215**, 3552-3558.

McGowan, C. P., Baudinette, R. V. and Biewener, A. A. (2005). Joint work and power associated with acceleration and deceleration in tammar wallabies (*Macropus eugenii*). *J. Exp. Biol.* **208**, 41-53.

McGowan, C. P., Neptune, R. R. and Kram, R. (2008). Independent effects of weight and mass on plantar flexor activity during walking: implications for their contributions to body support and forward propulsion. *J. Appl. Physiol.* **105**, 486-494.

McGuigan, M. P., Yoo, E., Lee, D. V. and Biewener, A. A. (2009). Dynamics of goat distal hind limb muscle–tendon function in response to locomotor grade. *J. Exp. Biol.* **212**, 2092-2104.

Medler, S. (2002). Comparative trends in shortening velocity and force production in skeletal muscles. *Amer. J. Physiol. Reg. Integr. Comp. Physiol.* **283**, R368-R378.

Nelson, F. E., Gabaldón, A. M. and Roberts, T. J. (2004). Force-velocity properties of two avian hindlimb muscles. *Comp. Biochem. Physiol. A Mol. Integr. Physiol.* **137**, 711-721.

Nishikawa, K. C., Monroy, J. A., Uyeno, T. E., Yeo, S. H., Pai, D. K. and Lindstedt, S. L. (2012). Is titin a 'winding filament'? A new twist on muscle contraction. *Proc. R. Soc. B Biol. Sci.* **279**, 981-990.

Olson, J. M. and Marsh, R. L. (1998). Activation patterns and length changes in hindlimb muscles of the bullfrog *Rana catesbeiana* during jumping. *J. Exp. Biol.* **201**, 2763-2777.

Pollock, C. M. and Shadwick, R. E. (1994a). Allometry of muscle, tendon, and elastic energy storage capacity in mammals. *Amer. J. Physiol. Reg. Integr. Comp. Physiol.* **266**, R1022-R1031.

Pollock, C. M. and Shadwick, R. E. (1994b). Relationship between body mass and biomechanical properties of limb tendons in adult mammals. *Amer. J. Physiol. Reg. Integr. Comp. Physiol.* **266**, R1016-R1021.

Preuschoft, H. (2002). What does "arboreal locomotion" mean exactly and what are the relationships between "climbing", environment and morphology? *Z. Morphol. Anthropol.* **83**, 171-188.

Rack, P. M. H. and Westbury, D. R. (1969). The effects of length and stimulus rate on tension in the isometric cat soleus muscle. *J. Physiol.* **204**, 443-460.

Roberts, T. J. and Azizi, E. (2011). Flexible mechanisms: the diverse roles of biological springs in vertebrate movement. *J. Exp. Biol.* **214**, 353-361.

Roberts, T. J., Marsh, R. L., Weyand, P. G. and Taylor, C. R. (1997). Muscular force in running turkeys: the economy of minimizing work. *Science* **275**, 1113-1115.

Roberts, T. J., Higginson, B. K., Nelson, F. E. and Gabaldón, A. M. (2007). Muscle strain is modulated more with running slope than speed in wild turkey knee and hip extensors. *J. Exp. Biol.* **210**, 2510-2517.

Russell, A. P. and Bels, V. (2001). Digital Hyperextension in *Anolis sagrei*. *Herpetologica* **57**, 58-65.

Schmidt, A. and Fischer, M. S. (2010). Arboreal locomotion in rats–the challenge of maintaining stability. *J. Exp. Biol.* **213**, 3615-3624.

Shadwick, R. E. and Syme, D. A. (2008). Thunniform swimming: muscle dynamics and mechanical power production of aerobic fibres in yellowfin tuna (*Thunnus albacares*). *J. Exp. Biol.* **211**, 1603-1611.

Shadwick, R. E., Steffensen, J. F., Katz, S. L. and Knower, T. (1998). Muscle dynamics in fish during steady swimming. *Amer. Zool.* **38**, 755-770.

Spezzano, L. C., Jr and Jayne, B. C. (2004). The effects of surface diameter and incline on the hindlimb kinematics of an arboreal lizard (*Anolis sagrei*). *J. Exp. Biol.* **207**, 2115-2131.

Wells, J. B. (1965). Comparison of mechanical properties between slow and fast mammalian muscles. *J. Physiol.* **178**, 252-269.

Wickler, S. J., Hoyt, D. F., Biewener, A. A., Cogger, E. A. and De La Paz, K. L. (2005). *In vivo* muscle function vs speed II. Muscle function trotting up an incline. *J. Exp. Biol.* **208**, 1191-1200.

Zaaf, A., Herrel, A., Aerts, P. and De Vree, F. (1999). Morphology and morphometrics of the appendicular musculature in geckoes with different locomotor habits (Lepidosauria). *Zoomorphology* **119**, 9-22.

Zar, J. H. (1999). *Biostatistical Analysis*. Upper Saddle River: Prentice Hall.

Table S1. Hind limb muscle and tendon morphology for *Anolis equestris*.

		Individual						
	Variable	1	2	3	4	5	6	7
External morphology	Body mass	63.92	60.33	78.32	74.58	40.35	52.89	39.12
	SVL	15.1	15	16.1	15	12.5	14.1	12.3
	Total length	39	37.7	46.1	29.5	28.5	38.4	34.6
	Humerus length	2.5	2.5	2.5	2.1	2.4	2.7	2.1
	Radius length	2.3	2	2.5	2.1	2	2.1	1.7
	Metacarpal length	0.9	0.9	1	0.8	0.6	0.6	0.6
	3rd finger length	1	1	1	0.9	0.8	1	0.9
	Femur length	3.5	3	3.3	2.8	2.7	2.6	2.6
	Tibia length	3.1	2.9	3.4	2.8	2.9	2.9	2.5
	Metatarsal length	1.9	2	2.1	1.7	1.5	1.8	1.3
	4th toe length	1.8	1.9	2.1	1.9	1.5	1.7	1.4
Puboischiotibialis	Fascicle length	3.3	3.8	3.1	3.7	3.3	3.4	2.8
	Tendon length	0.2	0.2	0.5	0.4	0.2	0.5	0.4
	Tendon mass for length=0.2cm	0.0018	0.0029	0.0028	0.001	0.001	0.0013	0.0018
	Insertion on tibia (cm from knee)	0.3-0.7	0.4-0.8	0.5-0.9	0.3-0.6	0.5-0.8	0.4-0.8	0.3-0.6
	Origin on pelvic girdle (cm from hip)	0.5	0.7	0.4	0.6	0.6	0.6	0.4
	Mass	0.3058	0.3096	0.5094	0.404	0.2323	0.3547	0.2253
Flexor tibialis internus	Fascicle length	3	2.7	2.6	2.5	2.4	2.2	2
	Tendon length	0.2	0.2	0.5	0.4	0.2	0.5	0.4
	Tendon mass for length=0.2cm	0.0018	0.0029	0.0028	0.001	0.001	0.0013	0.0018
	Insertion on tibia (cm from knee)	0.7	0.8	0.9	0.6	0.8	0.8	0.6
	Mass	0.1191	0.1127	0.1737	0.1533	0.0863	0.1234	0.0742
Flexor tibialis externus	Fascicle length	3.1	3	2.9	2.7	2.5	2.6	2.3
	Insertion on tibia (cm from knee)	0.4	0.3	0.3	0.3	0.3	0.3	0.3
	Mass	0.1062	0.1399	0.2736	0.1896	0.1065	0.1474	0.1332
Pubofibularis	Fascicle length	2.5	2.5	2.7	2.5	2.3	2.3	2
	Insertion on fibula (cm from knee)	0.25	0.3	0.2	0.2	0.3	0.3	0.3
	MTU length	3.1	3.1	2.9	2.8	2.6	2.7	2.4
	Tendon mass for length=0.2cm	0.0004	0.0004	0.0005	0.0004	0.0006	0.0002	0.0008
	Mass	0.0668	0.0769	0.0987	0.1021	0.0514	0.068	0.0511
Femorotibialis pars ventralis	Avg fascicle length	1.7	1.7	1.9	2.1	1.4	1.6	1.3
	Insertion on tibia (cm from knee)	0	0	0	0	0	0	0
	Mass	0.0764	0.0741	0.1243	0.0875	0.0844	0.1224	0.0958
Ambiens pars ventralis	Fascicle length	2.6	2.6	2.4	2.4	2.4	2.3	1.9
	Insertion on tibia (cm from knee)	0.25	0.2	0.3	0.2	0.2	0.2	0.2
	Mass	0.1532	0.1916	0.2912	0.2202	0.1437	0.2102	0.1532

Ambiens pars dorsalis	Fascicle length	2.2	2	2.5	2.3	1.4	1.8	1.4
	Insertion on tibia (cm from knee)	0.25	0.2	0.3	0.2	0.2	0.2	0.2
	Tendon length	0.9	1	0.8	0.7	0.6	0.7	0.7
	Tendon mass for length=0.3cm	0.009	0.0063	0.004	0.0041	0.0029	0.003	0.0017
	Mass	0.1555	0.1522	0.223	0.1768	0.0939	0.1643	0.1169
Iliofibularis	Fascicle length	2.9	3	3.3	2.7	2.7	2.7	2.3
	Insertion on fibula (cm from knee)	0.6-0.8	0.7-0.9	0.9-1.1	0.6-0.8	0.5-0.7	0.5-0.7	0.4-0.6
	Mass	0.1791	0.1764	0.2788	0.223	0.1333	0.2187	0.1536
Ilioischiotibialis	Fascicle length	2.4	2.3	2.2	2.2	2	2	1.7
	Insertion on tibia (cm from knee)	0.7	0.7	0.6	0.6	0.6	0.6	0.5
	MTU length	2.8	2.7	2.5	2.7	2.5	2.5	2.1
	Tendon mass for length=0.2cm	0.0007	0.0007	0.0003	0.0004	0.0003	0.0004	0.0002
	Mass	0.1247	0.1044	0.174	0.1645	0.0789	0.1318	0.1056
Femorotibialis pars dorsalis	Fascicle length	1	1	1.1	1.1	1.1	1.1	1.1
	Insertion on tibia (cm from knee)	0	0	0	0	0	0	0
	Pennation angle	28	24	25	20	22	25	25
	Mass	0.1718	0.1392	0.241	0.1301	0.1151	0.1919	0.1427
Adductor femoris	Fascicle length	1.8	1.7	1.8	1.7	1.4	1.4	1.4
	Pennation angle	12	12	11	13	14	13	14
	Mass	0.1949	0.2236	0.2985	0.2688	0.1575	0.2854	0.2046
Ilioischiofibularis	Fascicle length	1.4	1.4	1.4	1.4	1.4	1.4	1.4
	Insertion on fibula (cm from knee)	0.4	0.4	0.4	0.4	0.4	0.4	0.4
	MTU length	2.2	2.2	2.2	2.4	2.2	2.1	2.2
	Tendon mass for length=0.3cm	0.0002	0.0002	0.0004	0.0006	0.0002	0.0005	0.0001
	Pennation angle	10	10	10	10	10	10	10
	Mass	0.0696	0.0472	0.0715	0.1022	0.0457	0.0637	0.0927
Tibialis anterior	Fascicle length	1.3	1.2	1.2	1.2	1.1	1.1	1
	Insertion on metatarsals (cm from ankle)	0.1-0.3	0.1-0.3	0.1-0.3	0.1-0.3	0.1-0.3	0.1-0.3	0.1-0.3
	Pennation angle	5	7	9	9	8	9	9
	Mass	0.0795	0.0876	0.098	0.0903	0.0512	0.1091	0.0693
Flexor digitorum communis	Fascicle length	1.3	1.4	1.3	1.2	1.1	1.1	1.1
	Insertion on metatarsals (cm from ankle)	0.2	0.2	0.2	0.2	0.2	0.2	0.2
	MTU length	1.5	1.6	1.5	1.5	1.5	1.7	1.5
	Tendon mass for length=0.3cm	0.0001	0.0013	0.0019	0.002	0.0014	0.0038	0.0008
	Mass	0.0226	0.0458	0.0544	0.0501	0.0347	0.1415	0.0323
Peroneus longus	Fascicle length	2.1	1.9	2.1	1.8	1.7	1.6	1.6
	MTU length	2.9	2.9	2.9	2.7	2.6	2.7	2.4
	Insertion on metatarsals (cm	0.3	0.3	0.4	0.4	0.4	0.3	0.2

	from ankle)							
	Tendon mass for length=0.45cm	0.0011	0.0015	0.0015	0.0013	0.0009	0.0005	0.0014
	Mass (g)	0.0462	0.0532	0.0708	0.0435	0.0312	0.0587	0.0494
Peroneus brevis	Fascicle length	0.5	0.5	0.5	0.5	0.5	0.5	0.5
	MTU length	2.8	2.4	2.4	2.2	1.9	2	1.9
	Insertion on metatarsals (cm from ankle)	0.1	0.1	0.1	0.1	0.1	0.1	0.1
	Tendon mass for length=0.3cm	0.001	0.0016	0.002	0.0013	0.0009	0.0005	0.0008
	Pennation angle	15	17	15	18	13	18	16
	Mass	0.0491	0.0481	0.0746	0.0585	0.0359	0.059	0.0465
Extensor digitorum longus	Fascicle length	2.6	2.3	2.2	2	1.9	2	1.9
	Femoral tendon length	1.2	1.4	1.2	1	1	1	0.9
	Mass femoral tendon for length=0.25cm	0.0004	0.0003	0.0008	0.0004	0.0004	0.0007	0.0006
	Origin on femur (cm from knee)	0.1	0.1	0.1	0.1	0.1	0.1	0.1
	MTP tendon length	0.9	1.2	1	0.9	0.9	0.8	0.8
	Mass MTP tendon for length=0.3	0.0004	0.0005	0.0008	0.0004	0.0003	0.0004	0.0007
	Insertion on metatarsals (cm from ankle)	0.3	0.5	0.6	0.4	0.3	0.4	0.4
	Mass	0.0497	0.0648	0.0781	0.0695	0.0366	0.0704	0.0753
Gastrocnemius pars fibularis pars minor	Fascicle length	1.4	1.2	1.2	1.2	1	1	1
	Insertion on metatarsals (cm from ankle)	0.4	0.4	0.4	0.4	0.4	0.4	0.4
	Origin on femur (cm from knee)	0.2	0.4	0.3	0.4	0.3	0.3	0.3
	Pennation angle	14	12	14	14	13	15	13
	MTU length	3.3	3.5	3.3	2.9	2.5	2.8	2.6
	Tendon mass for length=0.3cm	0.003	0.0027	0.0024	0.0034	0.0022	0.001	0.0019
	Mass	0.1282	0.1331	0.1723	0.1729	0.0874	0.1228	0.1067
Gastrocnemius pars fibularis pars major	Fascicle length	2.2	2.3	2.1	2.2	2	2.2	2.1
	Insertion on metatarsals (cm from ankle)	0.4	0.4	0.4	0.4	0.4	0.4	0.4
	Origin on femur (cm from knee)	0.2	0.4	0.3	0.4	0.3	0.4	0.3
	MTU length	3	3.2	3	2.9	2.5	2.7	2.5
	Tendon mass for length=0.3cm	0.0044	0.0043	0.0084	0.0057	0.0032	0.006	0.0026
	Mass	0.1303	0.1496	0.2877	0.2237	0.0955	0.1784	0.1418
Caudofemoralis longus	Muscle length	6.2	6.5	6.8	7.1	5.7	5.8	5.5
	Avg fascicle length	1.9	2.1	2	1.9	1.8	1.8	1.8
	MTU length	6.8	7.1	7.3	7.6	6.2	6.3	6

Pennation angle	20	17	20	16	15	15	15
Femoral tendon mass for length=0.5cm	0.0041	0.0055	0.0044	0.0052	0.0031	0.0045	0.0062
Mass	0.7325	0.8505	1.233	1.0221	0.5983	0.7314	0.9384

SVL, snout-vent length; MTU, muscle-tendon unit; MTP, metatarsalphalangeal; Avg, average.
All lengths given in cm; all masses given in g.

Table S2. Mean muscle-tendon unit (MTU) length and tendon length change in mm and as a percentage of MTU length for all the hind limb muscles of the femur and crus that have tendons.

Muscle	Tendon length change (mm)	MTU length (mm)	Tendon length change (% of MTU length)
Puboischiotibialis	0.014	36.8	0.038
Flexor tibialis internus	0.008	2.8	0.294
Pubofibularis	0.026	28	0.094
Ambiens pars ventralis	0.017	31.4	0.053
Ambiens pars dorsalis	0.016	27.1	0.060
Ilioischiotibialis	0.048	25.4	0.189
Ilioischiofibularis	0.191	22.1	0.863
Flexor digitorum communis	0.018	15.4	0.115
Peroneus longus	0.051	27.3	0.187
Peroneus brevis	0.029	22.3	0.132
Extersor digitorum longus	0.076	41.6	0.182
Gastrocnemius pars fibularis pars minor	0.038	29.9	0.125
Gastrocnemius pars fibularis pars major	0.011	28.3	0.037
Caudofemoralis longus	0.069	67.6	0.103

Table S3. Loadings from a discriminant function (DF) analysis (Wilks' Lambda F=1.87, p=0.0466) of hind limb joint angles in *Anolis equestris*. As only DF1 was significant (p=0.0466), DF2 (p=0.97) is not shown.

Variable	DF1 (94.6%)
Femur depression angle (ES)	**0.9431**
Max. swing femur depression angle	**0.9417**
Mid swing femur depression angle	**0.9311**
Femur rotation angle (ES)	**-0.9104**
Knee angle (FF)	**-0.9083**
Max. femur depression angle	**0.8611**
t. max. femur rotation angle (% swing)	**0.8152**
Femur depression angle (MS)	**0.7668**
t. min. knee angle (% stance)	**-0.7656**
Pelvic girdle rotation angle (MS)	**0.4865**
Pelvic girdle rotation angle (ES)	**0.3729**
Max. swing ankle angle	0.0684

Loadings with a magnitude ≥ 0.3 are in bold.
Percentage of variation explained by DF1 axis is indicated in parentheses.
FF, footfall; MS, mid stance; ES, end of stance; T, time; Max., maximum; Min., minimum.

Table S4. Loadings from a discriminant function (DF) analysis (Wilks' Lambda F=2.04, p=0.028) of hind limb angular velocities in *Anolis equestris*. As only DF1 (p=0.028) was significant, DF2 (p=0.24) is not shown.

Variable	DF1 (64.3%)
Max. swing knee angle velocity (residuals)	**0.8093**
Mid swing knee angle velocity	**0.8087**
Avg. swing femur rotation velocity (residuals)	**-0.8081**
Avg. swing knee angle velocity	**0.7475**
Max. swing ankle angle velocity (residuals)	**0.7429**
Avg. stance knee angle velocity	**-0.665**
Avg. stance ankle angle velocity (residuals)	**-0.6262**
Max. stance femur depression velocity	0.1951
Femur depression velocity (MS)	0.1631
Min. swing femur depression velocity	-0.1519
Avg. stance femur depression velocity	-0.1331
Min. swing ankle angle velocity (residuals)	0.1128

Loadings with a magnitude ≥ 0.3 are in bold.
Percentage of variation explained by DF1 axis is indicated in parentheses.
Variables that were loaded as residuals because they regressed significantly with body speed are indicated in parentheses.
MS, mid stance; Max., maximum; Min., minimum; Avg., average.

Table S5. Hind limb joint angle and angular velocity variables that loaded heavily (≥ 0.3) on the first axis of discriminant function analyses (Fig. 3, Tables 3,4).

	Perch Diameter	
	Narrow	Broad
Joint Angle		
Femur depression angle (ES)	38.43±2.30	9.49±1.68
Max. swing femur depression angle	40.23±2.45	9.42±1.83
Mid swing femur depression angle	33.53±2.75	-3.92±2.33
Femur rotation angle (ES)	50.50±2.38	76.24±1.39
Knee angle (FF)	48.36±3.23	88.77±2.09
Max. femur depression angle	42.85±2.28	19.73±2.50
t. max. femur rotation angle (% swing)	45.03±5.19	9.88±2.17
Femur depression angle (MS)	35.68±2.83	11.50±2.85
t. min. knee angle (% stance)	9.77±2.85	42.28±4.75
Pelvic girdle rotation angle (MS)	-2.67±1.83	-12.72±2.94
Pelvic girdle rotation angle (ES)	-0.67±2.62	-8.57±2.78
Joint angular velocity		
Max. swing knee angle velocity	308.01±75.08	955.63±140.35
Mid swing knee angle velocity	-480.66±76.01	247.44±115.90
Avg. swing femur rotation velocity	-45.80±19.34	-180.21±20.58
Avg. swing knee angle velocity	-422.71±66.36	17.11±47.26
Max. swing ankle angle velocity	276.54±84.58	892.83±127.37
Avg. stance knee angle velocity	217.19±37.67	11.00±26.16
Avg. stance ankle angle velocity	247.13±46.68	96.46±28.11

FF, footfall; MS, mid stance; ES, end of stance; t., time; Max., maximum; Min., minimum; Avg., average.
Velocities are in degrees s^{-1}; values are means ± s.e.m.